Energy Exchange Network Model Demonstrates Protein Allosteric Transition: An Application to an Oxygen Sensor Protein

Kunitaka OTA[1] and Takahisa YAMATO*[1,2]

[1]*Graduate School of Science, Nagoya University, Furo-cho, Chikusa-ku, Nagoya 464-8602, Japan*

[2]*Institute of Genetics and Molecular and Cellular Biology, University of Strasbourg, 1 rue Laurent Fries Parc d'Innovation 67404 Illkirch, Cedex, France*

Correspondence: yamato@nagoya-u.jp

ABSTRACT: The effects of ligand binding on an oxygen sensor protein, FixLH, were investigated by molecular dynamics (MD) simulation. To illustrate the network of residue interactions in the deoxy, oxy, and carbomonoxy states of FixLH, we employed the energy exchange network (EEN) model in which residue interactions were evaluated in terms of local transport coefficients of energy flow. As a result, the difference map of EEN between the deoxy and oxy (deoxy and carbomonooxy) states clearly demonstrated the allosteric transition, although the structural changes by ligand binding are small. It is known that the FixLH forms a homodimer in solution, although neither O_2 nor CO-binding exhibits cooperativity. Therefore, we conjectured that the primary event after ligand binding occurs essentially at the monomer level, and it is subsequently followed by quaternary structural changes. The difference EEN maps showed that two regions, (A) the junction between the coiled-coil linker and the sensor domain and (B) potential dimer interface, experienced considerable change of the energy transport coefficients, indicating that these two regions play important roles in quaternary structural changes and signal transduction in response to ligand binding.

INTRODUCTION

Within a thermally fluctuating protein molecule under physiological conditions, amino acid residues are interacting with each other by exchanging energies between them.[1–7] In response to external stimulus, a protein molecule undergoes structural/dynamical changes in performing its biological function.[8–18] To understand the underlying mechanisms of protein functions, it would be helpful to analyze the rearrangement of the residue interaction network associated with such structural/dynamical changes.

Energy transport in a native protein occurs highly anisotropically,[19–24] and the spatial pattern of such energy flow differs from protein to protein. Recently, further examinations with MD simulation have led to a scaling relation between energy transport rates across non-bonded contacts and the thermal fluctuations of these contacts.[25,26] We are mainly concerned with the characterization of such anisotropic energy transport, which is illustrated by local transport coefficients calculated based on linear response theory, and how such local properties are demonstrated as a residue interaction network that mediates energy dynamics in the protein.[27,28] It is known that the local energy transport coefficient is sensitive not only to structural changes but also

to subtle changes in dynamics and conformational fluctuations.[26] In the previous study, we applied this method to study the underlying mechanism of the hidden dynamic allostery of a small globular protein, PDZ3.[28] It is counterintuitive that the removal of its C-terminal helix is known to decrease ligand binding affinity by 21-fold without changing the overall protein structure. As a result of our calculations, we demonstrated that its C-terminal helix constituted an essential part of the interaction network, indicating that the helix plays an important role in mediating energy flow within the native conformation of PDZ3.

In this study, we investigated the allosteric transition mechanism of a gas sensor protein. The molecular and cellular basis of environmental sensing has been one of the fundamental issues in life science. For example, two-component systems (TCS) enable living organisms to detect physical/chemical stimuli in their environment.[29, 30] TCS typically consists of a histidine kinase (HK) and a response regulator (RR), and HK consists of a kinase domain and a sensor domain. Thus, the kinase-sensor interaction plays central roles in signal transduction of TCS. The kinase-sensor complex structures, however, are rarely provided at high resolutions, and it is known that the structural change

of the sensor domain induced by ligand binding is often small.[31] Accordingly, the molecular mechanism of the signal transduction of TCS has been not yet fully understood yet. Here, we investigated the primary stage of signal transduction mechanism of the sensor domain of an O_2-dependent kinase, FixL derived from *B. japonicum* (Figure 1), based on the computational analysis of inter residue energy flow. The gene topology of *B. Japonicum* FixL is shown in Figure 1A. It shows tandem PAS (Per-Arnt-Sim) consisting of PAS-A and PAS-B, together with its histidine kinase domain. The kinase activity of FixL is suppressed by O_2 (CO) binding to its heme-containing sensor domain, FixLH, which corresponds PAS-B in Figure 1A. It is known that this protein forms a homodimer in solution. However, neither O_2 nor CO-binding to the homodimer exhibits cooperativity.[32] Ayers and Moffat suggested the importance of quaternary structural transitions with negligible free-energy changes in the signaling mechanism of PAS domains.[31] Recently, the architecture of the complete oxygen-sensing TCS was reported[33], which is consistent with rotary switch model[34, 35, 36]/in-line model[33, 37, 38, 39] in the literatures. They constructed a model based on solution scattering data. Like YF1 structure (Fig. 1C), the FixLH domain is connected to the kinase domain by a coiled-coil

linker. Importantly, recent studies of time-resolved X-ray solution scattering and electron-electron double resonance (ELDOR) demonstrated YF1 signal transduction mechanism via the coiled-coil by quaternary transitions.[40, 41, 42] Taking these observations into account, we can conjecture that FixL signal transduction occurs in three steps: (1) ligand binding to either one of the two monomers in the FixLH homodimer triggers the primary event at the "monomer level" without large structural changes, (2) this exercise substantial impacts on the homodimeric interface of FixLH and also on the junction with the coiled-coil liner. (3) As a result, quaternary structural changes[40, 41, 42] occur in the homodimer, and signal is transmitted to the histidine kinase domain via the coiled-coil linker. In this study, we have mainly focused on in the early stages from (1) to (2). Therefore, we took a bottom up approach and started our MD simulations with monomer FixLH, although it might be desirable to perform MD simulations with the dimeric form to study its molecular behaviors in a realistic manner, which is the subject of a future work. In addition, we have another reason why we performed monomer simulations. We are interested in the general and intrinsic properties of the PAS fold at the monomer level, including photoactive yellow protein[27 43 44 45 46 47] and others, and their responses to

external stimuli. Also, if we perform MD simulations for the dimeric form, it is not possible to distinguish between the ligand binding effect and the effect of monomer-monomer interaction via the dimer interface on the structural change of each FixLH monomer. To investigate the direct influence of ligand binding on the monomer structure, we performed MD simulations with monomer FixLH.

To evaluate the effect of O_2 (CO) binding to a FixLH monomer, we performed MD simulations of deoxy- and oxy- (carbomonoxy-) FixLH, and analyzed the difference of residue-residue interactions between the two states. As a result, we identified distinct clusters of surface residues that experienced significant changes of residue interactions, indicating these clusters mediates the crosstalk between FixLH and the kinase domain of FixL.

MATERIALS AND METHODS

Model Construction and Conformational Sampling. The deoxy, oxy, and carbomonoxy models of monomeric FixLH derived from *B. japonicum* were constructed based on the x-ray crystallographic structures (PDB codes 1xj3,[48] 1dp6,[49]

and 1xj2,[48] respectively) and denoted as FixLH, FixLH-O_2, and FixLH-CO, respectively. For each model, we included 102 residues from A155 to L256 and the N- and C-termini were caped with ACE (acetyl) and NME (N-methylamine) groups, respectively. The C-terminal helix beginning from T257 was excluded because it undergoes large fluctuations. For all of the three models, (H235) H162, H200, and H214 were treated as neutral residues with their (epsilon) delta nitrogen protonated. The fifth coordination site of the heme iron is occupied by the imidazole ring of H200, proximal histidine. The protonation states of all other ionizable residues were maintained in their standard states at pH = 7.0. Each model was immersed in a box of water molecules and the size of the box (the number of water molecules) were 72.6× 71.8×68.8, 74.1×69.2×68.8, and 72.6×71.8×68.9 $Å^3$ (9046, 8799, and 9086), for FixLH, FixLH-O_2, and FixLH-CO, respectively. To neutralize each system, we added 28 sodium and 24 cloride ions and the total number of atoms became, 28863, 28124, and 28985 for FixLH, FixLH-O_2, and FixLH-CO, respectively. Thus, the concentration of [NaCl] became 0.154 M.

The Amber 14 program[50] was used to perform MD simulations, with the ff14SB[51] and

TIP3P[52] force-field functions for the polypeptide chain and waters. We tuned the force-field parameters for FixLH, FixLH-O_2, and FixLH-CO based on the resources available in the amber force field parameter database (http://research.bmh.manchester.ac.uk/bruyce/amber).[53] Our parameters are available via the website (http://www.comp-biophys.com/resources/force-field/o2-sensor/o2-sesor.zip). Following the procedure described in Takayanagi et al.,[22] we modified the bond (angle) patameters for FE–N_heme, FE–N_his, (N_heme–FE–N_his, N_heme–FE–N_his, N_heme–FE–N_heme), based on the parameters developed by Henry et al.[54] The partial atomic charges of the H200–heme and H200–heme–ligand complex were calculated by using the Gaussian 03 and Molden programs,[55,56] and RESP fitting by the RED program.[57]

We employed a periodic boundary condition for each system, and the long-range Coulomb interactions were evaluated using the particle mesh Ewald method. For the nonbonded particle-particle interactions were evaluated using the cut-off length of 9.0 Å. The positions of the hydrogen atoms were optimized before conformational sampling, and then the side-chain atoms were optimized with positional restraints of 99.9

(kcal/mol)/Å^2 on the backbone atoms (N, C_α, C, O). Finally, the positions of the main chain atoms were optimized with positional restraints of 2.0 (kcal/mol)/Å^2.

The time step for the MD simulations was set as 2.0 fs, and the SHAKE constraints were applied for all covalent bonds involving a hydrogen atom. The temperature of each system was then increased from 0.1 to 300 K for 50 ps by performing constant temperature, constant volume (*NVT*) MD simulations with the relaxation time of 0.1 ps and a positional restraint of 2.0 (kcal/mol)/Å^2 on the backbone atoms. Before the heating process, a Maxwell-Boltzmann distribution of initial atomic velocities was generated at 0.1 K. We continued another *NVT* MD simulation at T = 300 K for 50 ps with keeping the same positional restraints, then switched off the positional restraints, and a Langevin MD simulation was performed with a collision frequency of 2.0 ps^{-1} for 200 ps at T = 300 K. Finally isothermal-isobaric (*NPT*) MD simulation was performed for 700 ps at T = 300 K, P = 0.987 atm, and the final conformation was saved for further use (Fig. 2).

Starting from the end point of the previous simulations, we performed 20 independent *NPT* MD simulations for 55 ns at T = 300 K and P = 0.987 atm with different velocity distributions. From the last 5.0 ns of each of these 20 trajectories, 10 snapshots of atomic

coordinates and velocities were extracted every 0.5 ns. As a result, we obtained 200 (= 20×10) independent initial conditions for further calclations of inter-atomic energy flow. Finally, we performed N_{traj} = 200 (= 20×10) constant volume, constant energy (*NVE*) MD simulations for 1 ns and atomic coordinates and velocities were saved every 10 fs.

Inter-Residue Energy Flow Calculations. Using the CURP program,[28] we calculated the inter-residue energy flow, *J*, using the N_{traj} *NVE* MD trajectories. Here we briefly summarize how to analyze: At each time point, t ($0 < t < 1$ ns), *J* is calculated using the following equations:

$$J^k_{i\leftarrow j}(t) = \frac{1}{2}(\mathrm{v}_{\boldsymbol{i}} \cdot \boldsymbol{F_{ij}} - \mathrm{v}_{\boldsymbol{j}} \cdot \boldsymbol{F_{ji}}) \quad \ldots (1)$$

and

$$J^k_{A\leftarrow B}(t) = \sum_{i\,\in\, A}^{N_A} \sum_{j\,\in\, B}^{N_B} J^k_{i\leftarrow j}(t), \quad \ldots (2)$$

where N_A (N_B) are the total number of sidechain atoms in residues A (B), and sidechain atom i (j) are taken from residues A (B); $\boldsymbol{v}_i$ is the velocity of the ith atom, and $\boldsymbol{F}_{ij}$ is the pairwise interatomic force[58] from atom j to i; and index k distinguishes different trajectories (k = 1, 2, …, 200). In this study, we considered only nearby residue pairs so that the shortest interatomic distance between each pair was less than 6 Å and neglected other pairs. Consequently,

$$L^k_{AB} = \frac{1}{RT}\lim_{\tau\to\infty} \int_0^\tau \left\langle J^k_{A\leftarrow B}(0) J^k_{A\leftarrow B}(t)\right\rangle dt, \quad \ldots(3)$$

and

$$\left\langle J^k_{A\leftarrow B}(0) J^k_{A\leftarrow B}(t)\right\rangle = \frac{1}{N}\sum_{t_i\,=\,0}^{N} J^k_{A\leftarrow B}(t_i) J^k_{A\leftarrow B}(t_i + t). \quad \ldots(4)$$

Here, R and T are the gas constant and absolute temperature, respectively. If the upper limit of the time integral in eq. (3) is sufficiently greater than the characteristic time scale for vibrational energy transfer, the limit operation is unnecessary. In this study, we set τ = 50 ps and N = 5000 and L^k_{AB} was averaged over the N_{traj} trajectories to obtain,

$$L_{AB} = \frac{1}{N_{traj}} \sum_{k=1}^{N_{traj}} L^k_{AB}. \quad \ldots(5)$$

Hereafter, $D \equiv RT \times L_{AB}$ is referred to as inter-residue energy conductivity.

RESULTS AND DISCUSSION

Reorganization of the Network of Residue-Residue Interactions upon O_2 Binding.

We show EENs of FixLH, FixLH-O_2, and FixLH-CO respectively in Figs. S1, 2 and 3, indicating that the entire molecule is connected via the networks of residue interactions. To analyze the effect of O_2 binding on FixLH, we considered 1386 pairs of residues closer than the cut-off distance of 6Å and compared the difference between EENs of FixLH-O_2 and FixLH (Fig. 3). Note that the distance between each residue pair was defined as the shortest interatomic distance between the pair. We calculated the differences of Ds, hereafter denoted as ΔD, of FixLH-O_2 from those of FixLH. As a result, its average ($\overline{\Delta D}$) and standard deviation (σ) were -4.5×10^{-6} and 1.8×10^{-3} [(kcal/mol)/fs], respectively.

Next, we illustrate the difference-EEN map, hereafter denoted as ΔEEN(O_2), for the

O_2 binding based on ΔD. The residue pairs with strengthened (weakened) interactions by the O_2 binding were defined by those with ΔD greater (less) than $\overline{\Delta D} + (-)\,\sigma$. We clearly see that the effect O_2 binding is not localized to the heme pocket but propagated throughout the entire molecule.

Analysis of Surface Sites in EEN. In this study, we focused our attentions on (A) the junction between the sensor domain and the coiled-coil linker and (B) potential dimer interface. (A): In our model, the C-terminal helix was truncated, and the region near the C-terminal end of the Iβ strand is connected to the coiled-coil linker and this region is also *exposed* on the surface. (B): We consider that the dimer interface is important for quaternary structural changes, and the surface *exposed* residues in the monomeric unit can be in contact with the other monomer on the interface. In other words, buried residues within the sensor domain can directly interact with neither the other sensor domain nor the coiled-coil linker.

In this section, we identify the surface exposed residues that experience considerably large $|\Delta D|$. We conjectured that these residues are candidates for key residues responsible for either quaternary structural changes or signal transduction via the coiled-coil linker.

We calculated[59] the solvent accessibility[60] of each amino acid residue and a given residue was defined as exposed if its solvent accessibility was greater than 50 %. The total number of the surface sites was 15 in Fig. 3. Considering the tertiary structure of FixLH, these sites were clustered into two distinct groups, *i.e.,* cluster *1* and *2*. Interestingly, cluster *1* and *2* are completely separated in the network graph shown in Fig. 3. The cluster *1* mainly consists of the sites in the Fα helix, FG-loop, and both ends of HI-loop, while cluster *2* near *N* and *C* termini. The roles of each cluster will be discussed in relation to the functional mechanism later.

Note that the choice of 50% threshold is often used to distinguish between exposed residues and buried ones. There are four residues (T230, L167, P233, and T210) with solvent accessibility falling within the range of plus minus 1% around 50% and five more residues (R227, S202, D201, D255, and S243) within the range of plus minus 2% around 50%. Among them, T210 and D255 are surface sites labeled with closed circles in Figs. 3 and 4.

Effect of CO Binding. It is known that the kinase activity of FixL is also inhibited by CO binding, although the inhibition by CO is weaker than that by O_2.[61] Therefore, we

expect that we can get some hints about the signal transmission mechanism by a comparison between O_2 and CO binding effects. To analyze the effect of CO binding, we performed the difference-EEN analysis for FixLH-CO and FixLH in the same manner as described before. We considered 1404 pairs of residues within the cut-off distance of 6Å and compared the difference between EENs of FixLH-CO and FixLH (Fig. 4). We calculated the differences of *D*s of FixLH-CO from those of FixLH. As a result, the values of $\overline{\Delta D}$ and σ were 1.8×10^{-5} and 6.3×10^{-4} [(kcal/mol)/fs], respectively. By comparing Figs. 3 and 4, we clearly see that the difference map, ΔEEN(CO), is sparser than ΔEEN(O_2). Accordingly, the total number of surface sites in ΔEEN(CO) decreased to 11, and all of these sites, except for T230, were contained in the 15 sites previously found in ΔEEN(O_2). It is likely that these observations are somehow related to the fact that the inhibitory effect by CO is weaker than that by O_2.

Structural Changes and Difference EEN Maps. In this section, we investigate how are the structural changes of FixLH reflected on ΔEEN(O_2) and ΔEEN(CO), focusing on the four different regions: (1) R206, (2) FG-loop (T211-G219), (3) R220, and (4) L236 and I238.

(1) The R206 side chain, which is located near H204 and the propionate side chain of the heme group, forms hydrogen bond with D212. The orientation of the R206 side chain is changed by O_2 binding to FixLH. On the other hand, such structural change does not occur by CO binding. Accordingly, we found R206 in $\Delta EEN(O_2)$, whereas we do not in $\Delta EEN(CO)$. Importantly, it is indicated that R206 involves in the signal transduction of FixL because the R206A mutant exhibits weaker inhibition of kinase activity.[62]

(2) This loop contains amino acid residues, H214, I215, and I216, that are in direct interaction with the heme group, and these interactions can be affected by the ligand binding. Structural comparison shows that the polypeptide backbone of the FG-loop and the residues attached to its both ends, *i.e.,* T209 and T210 (R220) on the N(C)-terminal side, are shifted by 1.0 ～ 1.8 Å by O_2 binding, whereas no such changes are induced by CO binding. Importantly, it is indicated that the FG-loop plays an important role in the signal transduction of O_2 binding to FixLH.[63–67]

(3) In deoxy-FixLH, R220 forms a hydrogen bond with the propionate side chain of the heme group. By the O_2 binding to FixLH, this hydrogen bond breaks and a new hydrogen bond is formed between O_2 and R220, which is reoriented inward to the heme pocket. On the other hand, no such structural changes are found for the CO-binding. We recognize considerable changes of the interaction network with R220 in $\Delta EEN(O_2)$, while no such change was found in $\Delta EEN(CO)$.

(4) These two residues constitute a so-called hydrophobic triad [64,68] with I215, and are located right above the ligand binding site, and thereby change their orientations and positions by the ligand binding to the heme group. Accordingly, we recognized

changes of the interaction network with these residues in both $\Delta EEN(O_2)$ and $\Delta EEN(CO)$.

Comparison between O_2 and CO Binding. We now compare the two maps, $\Delta EEN(O_2)$ and $\Delta EEN(CO)$, and examine the common/different parts between them. The common parts are shown in Fig. S4. In this map, we grouped the amino acid residues into three groups depending on underlying cause that possibly induced the interaction changes: (A) Conformational change of the heme group from domed to planer shape (orange). This conformational change is propagated through the H200 and T203 to Fα, Eα, and EF-loop. (B) Steric interaction with the ligand (cyan). Note that the color codes are different from those in Figs. 3, 4. The effect of ligand binding is mediated through L236 and I238, which are located right above the ligand binding site, to Hβ and Iβ. (C) The secondary effect of (A) and (B) (green). These parts, Cα, Dα, EF-loop, Gβ, GH-loop, and Iβ, are distant from the heme iron and the structural changes by ligand binding are very small. Therefore, it is indicated that changes of the interaction network were induced by the secondary effect of the above two causes (A) and (B).

Figure S5 illustrates the interaction changes that are specific to O_2 binding and not found for CO binding. The common parts between $\Delta EEN(O_2)$ and $\Delta EEN(CO)$ (see Fig. S4) are removed from $\Delta EEN(O_2)$ (Fig. 3). As described before, the structural change of FixLH by CO binding is much smaller than that by O_2 binding. Reorientation of the side chains of R206, R220 and the shift of the polypeptide backbone of FG-loop are induced by O_2 binding while such changes do not occur by CO binding. These differences are reflected in the map (Fig. S5). Taking all of these observations into account, it might be hypothesized that Fig. S4 represents essential network for the signal transduction, while

the network in Fig. S5 facilitates the efficient signal transmission.

Signal Transduction Mechanism. We introduce several models proposed by the experimental studies so far. We denote the FixLHs derived from *B. japonicum* and *S. meliloti* as BjFixLH and SmFixLH, respectively.

The first model is FG-loop switch model. As described before, this region undergoes structural changes by O_2 binding, the it is indicated that FG-loop is responsible for the signal transduction of FixL.[63–67] The second model emphasized the importance of Tyr-Glu hydrogen bonding. According to the ultraviolet resonance Raman spectroscopy studies of SmFixLH in the literatures, it is known that Y201, which corresponds to Y207 in BjFixLH, undergoes structural change by O_2 binding.[69,70] The third model is called domain swap model.[71,72] The fourth model is rotary switch model[34–36]/in-line model.[33,37,39,73] Our calculations support this model. In these models, there is no direct contact between the sensor and kinase domains. Recently, the architecture of the complete oxygen-sensing TCS was reported.[33] They constructed a model based on solution scattering data. Like YF1 structure (Fig. 1C), the FixLH domain is connected to the kinase domain by a coiled-coil linker, indicating that this linker mediates the allosteric signal transmission. Importantly, cluster *2* in ΔEEN(O_2) includes residues near C-terminus, indicating that the allosteric signal is mediated from FixLH to the kinase domain via these residues (Figs. 3, 5). Note that the C-terminal aspartic acid, D255, is highly conserved for FixLH sequences, indicating that this site is essential for signal transmission.[35] Near the C-terminal end, we recognize D255 and R254 in ΔEEN(O_2), while we do only D255 in ΔEEN(CO), indicating that the signal transmission via the C-terminal end to the coiled coil is more efficient for O_2 binding that that for CO binding. In either truncated FixLH[31]

or the full-length form of TCS,[33] FixLH formed a dimeric structure, and their interface was located in the Gβ, Hβ, and Iβ-strands,[31] indicating that intra-dimer communication between a pair of FixLH domains may occur upon O_2 binding through these β-strands. Importantly, we recognize E240 and E246 in these β-strands (Fig. 3), in line with the experimental observation.

Non-Equilibrium v.s. Equilibrium MD Simulation. To precisely study the allosteric transitions of proteins, careful long-time non-equilibrium simulations would be desirable[13 25]. Also, the time scales of the vibrational energy transfer and the allosteric transition are very different in general, indicating that the latter is not the direct outcome of the former. Nonetheless, the analysis of vibrational energy relaxation using equilibrium MD simulation is helpful to characterize the conformational/dynamical state of a protein. With this analysis, we can investigate what happens as a result of the allosteric transition, and which part of the molecule is important for the transition. We mainly focused on these problems in this study.

Recently, scaling relation has been observed between the local energy transport coefficient and the equilibrium fluctuations.[26] Importantly, using non-equilibrium MD simulation, Stock and coworkers reported the scaling relation between the energy transfer rate and the conformational fluctuations in their pioneering work.[25] Considering these observations into account, we can say that the analysis of the local energy transport coefficient based on equilibrium MD simulations inherently retains some essential features of the energy transfer rate that is derived from careful non-equilibrium MD simulation.

CONCLUSIONS

The effects of ligand binding on an oxygen sensor protein, FixLH, were investigated by theoretical computations. The energy exchange network (EEN) model successfully demonstrated the allosteric transition of FixLH domains for both O_2 and CO binding, although these structural changes are small. The difference EEN map between FixLH-CO and FixLH, (ΔEEN(CO)), was compared with that between FixLH-O_2 and FixLH, (ΔEEN(O_2)). As a result, ΔEEN(CO) was sparser than ΔEEN(O_2), in line with the experimental observation that the effect of CO-binding is weaker than that of O_2-binding. According to recent experimental reports on the FixL structures, the FixLH domain forms a dimeric form that is connected to the kinase domain through a coiled-coil linker[33,36], and the FixLH dimer interface was located at Gβ, Hβ, and Iβ-strands.[31] The difference EEN maps showed that two regions, (A) the junction between the coiled-coil linker and the sensor domain and (B) potential dimer interface, experienced considerable change of the energy transport coefficients, indicating that these two regions play important roles in quaternary structural changes and signal transduction in response to ligand binding.

Acknowledgements

The authors thank helpful discussion with Prof. Mizutani and Dr. Takemura. This work was supported by the Faculty Exchange Program between the University of Strasbourg and Nagoya University, and Grants-in-Aid from the Japan Research Institute of Industrial Science.

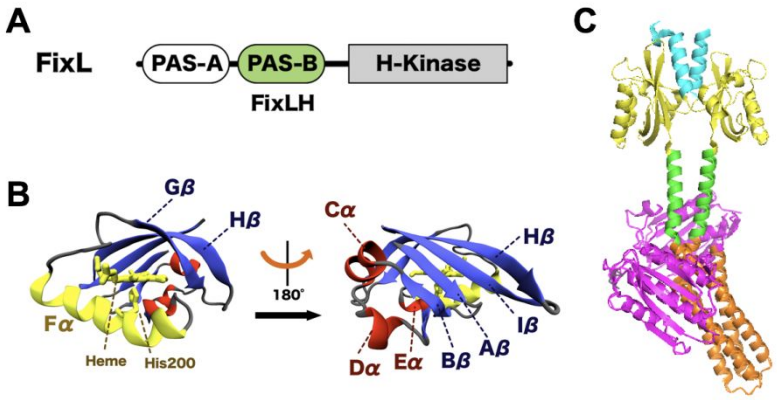

Figure 1. FixL gene, and crystal structures of FixLH and YF1. Topology of the FixL gene derived from *B. japonicum*, showing tandem PAS (Per-Arnt-Sim) domains consisting of PAS-A and PAS-B, together with its histidine kinase domain. The PAS-B domain is called FixLH and serves as an oxygen sensor. The x-ray structure of FixLH[48] (PDB id: 1xj3) are presented in two different orientations. This structure falls within the PAS-fold with five-stranded β sheet and four α helices. The secondary structural units are named Aβ, Bβ, Cα, Dα, Eα, Fα, Gβ, Hβ, and Iβ, from the N terminus, where α and β indicate the α-helix and β-strand, respectively. The heme group and the Fα helix, which is bound to the heme group is shown in yellow, the three other helices are in red, each β-strand is in purple, and the loops are in grey. Crystal structure of YF1 dimer[36]. Diensthuber et al. replaced the PAS-B domain of *B. japonicum* FixL with the light-oxygen-voltage (LOV) domain derived from *B. subtilis*. The histidine kinase part is consisted of dimerization/histidine phosphotransfer (DHp) and catalytic/ATP binding (CA) domains. The A'α (aa 1–22), LOV (aa 23–127), Jα (aa 128–147), DHp (aa 148–217), and CA (aa 218–375) domains are shown in cyan, yellow, green, magenta, and

orange, respectively. We see that the LOV dimer (yellow) is connected to the kinase domain by a coiled-coil linker (green).

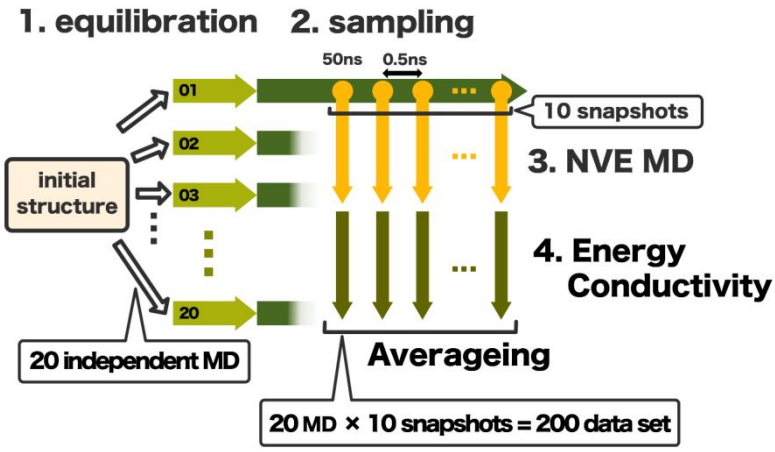

Figure 2. Calculation procedure. The calculations in this study consists of four stages: (1) thermal equilibration, (2) conformational sampling, (3) multiple *NVE* MD simulation, and (4) evaluation of inter-residue energy conductivity.

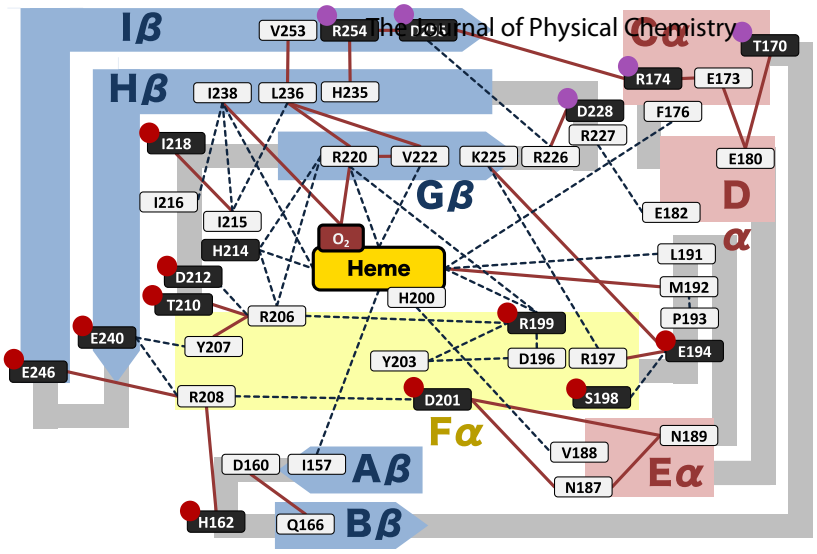

Figure 3. ΔEEN map between FixLH-O_2 and FixLH. Each amino acid residue is represented by a node shown as a rounded rectangle with its one letter code of amino acid and sequential number. The oxygen ligand is represented as a brown rounded rectangle. Residue pairs with ΔD greater (less) than $\overline{\Delta D}$ + (–) σ are connected by solid (broken) segments. Surface sites are represented as filled rectangles. These sites are separated into two different clusters, where cluster *1* and *2* are indicated by brown and purple circles, respectively.

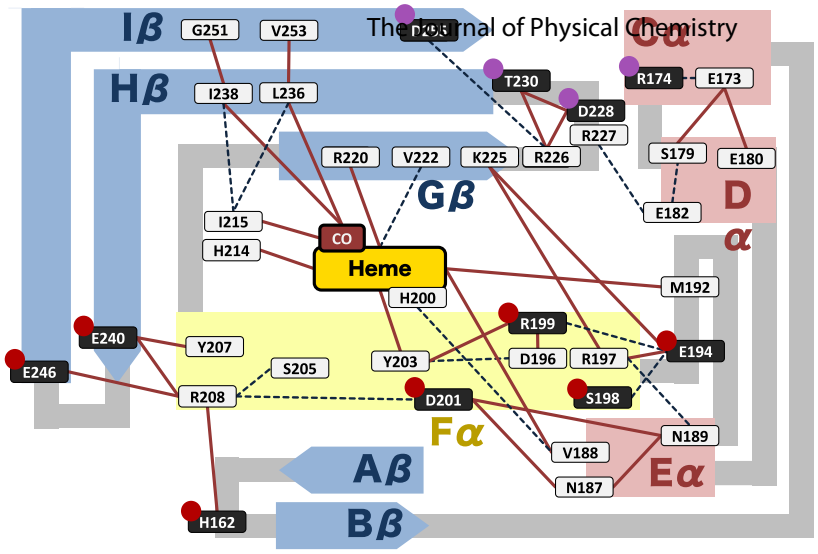

Figure 4. ΔEEN map between FixLH-CO and FixLH.

(see caption of Figure 3.)

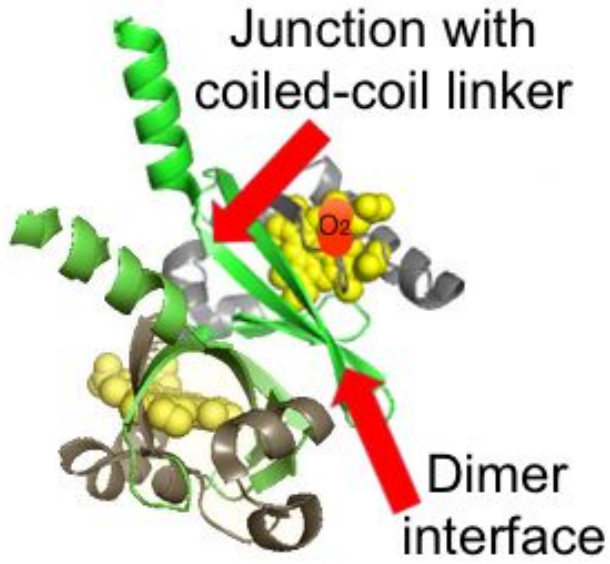

Figure 5. Schematic view of two important regions in the sensor domain.

REFERENCES

(1) Yamashita, S.; Mizuno, M.; Tran, D. P.; Dokainish, H.; Kitao, A.; Mizutani, Y. Vibrational Energy Transfer from Heme through Atomic Contacts in Proteins. *J. Phys. Chem. B* **2018**, *122*, 5877–5884.

(2) Hassan, S.; Schade, M.; Shaw, C. P.; Lévy, R.; Hamm, P. Response of Villin Headpiece-Capped Gold Nanoparticles to Ultrafast Laser Heating. *J. Phys. Chem. B* **2014**, *118*, 7954–7962.

(3) Kholodenko, Y.; Volk, M.; Gooding, E.; Hochstrasser, R. M. Energy Dissipation and Relaxation Processes in Deoxy Myoglobin after Photoexcitation in the Soret Region. *Chem. Phys.* **2000**, *259*, 71–87.

(4) Miller, R. J. D. Vibrational Energy Relaxation and Structural Dynamics of Heme Proteins. *Annu. Rev. Phys. Chem.* **1991**, *42*, 581–614.

(5) Sagnella, D. E.; Straub, J. E. Directed Energy “Funneling" Mechanism for Heme Cooling Following Ligand Photolysis or Direct Excitation in Solvated Carbonmonoxy Myoglobin. *J. Phys. Chem. B* **2001**, *105*, 7057–7063.

(6) Sagnella, D. E.; Straub, J. E.; Thirumalai, D. Time Scales and Pathways for

Kinetic Energy Relaxation in Solvated Proteins: Application to Carbonmonoxy Myoglobin. *J. Chem. Phys.* **2000**, *113*, 7702–7711.

(7) Yamato, T.; Saito, M.; Higo, J. Topographical Metric to Analyze the Thermal Fluctuations Of Protein Conformation. *Chem. Phys. Lett.* **1994**, *219* (1–2), 155–159.

(8) Tomita, A.; Sato, T.; Ichiyanagi, K.; Nozawa, S.; Ichikawa, H.; Chollet, M.; Kawai, F.; Park, S. Y.; Tsuduki, T.; Yamato, T.; et al. Visualizing Breathing Motion of Internal Cavities in Concert with Ligand Migration in Myoglobin. *Proc. Natl. Acad. Sci. U.S.A.* **2009**, *106*, 2612–2616.

(9) Tsuduki, T.; Tomita, A.; Koshihara, S.; Adachi, S.; Yamato, T. Ligand Migration in Myoglobin: A Combined Study of Computer Simulation and x-Ray Crystallography. *J. Chem. Phys.* **2012**, *136* (16).

(10) Itoh, K.; Sasai, M. Dynamical Transition and Proteinquake in Photoactive Yellow Protein. *Proc. Natl. Acad. Sci. U. S. A.* **2004**, *101*, 14736.

(11) Levantino, M.; Schirò, G.; Lemke, H. T.; Cottone, G.; Glownia, J. M.; Zhu, D.; Chollet, M.; Ihee, H.; Cupane, A.; Cammarata, M. Ultrafast Myoglobin

Structural Dynamics Observed with an X-Ray Free-Electron Laser. *Nat. Commun.* **2015**, *6*, 6772.

(12) Barends, T. R. M.; Foucar, L.; Ardevol, A.; Nass, K.; Aquila, A.; Botha, S.; Doak, R. B.; Falahati, K.; Hartmann, E.; Hilpert, M.; et al. Direct Observation of Ultrafast Collective Motions in CO Myoglobin upon Ligand Dissociation. *Science* **2015**, *350* (6259), 445–450.

(13) Buchenberg, S.; Sittel, F.; Stock, G. Time-Resolved Observation of Protein Allosteric Communication. *Proc. Natl. Acad. Sci.* **2017**, *114* (33), E6804--E6811.

(14) Aguayo-Ortiz, R.; Chávez-García, C.; Straub, J. E.; Dominguez, L. Characterizing the Structural Ensemble of γ-Secretase Using a Multiscale Molecular Dynamics Approach. *Chem. Sci.* **2017**, *8* (8), 5576–5584.

(15) Karathanou, K.; Bondar, A.-N. Dynamic Hydrogen-Bond Networks in Bacterial Protein Secretion. *FEMS Microbiol. Lett.* **2018**, *365* (13), fny124.

(16) Flechsig, H. Design of Elastic Networks with Evolutionary Optimized Long-Range Communication as Mechanical Models of Allosteric Proteins. *Biophys. J.* **2017**, *113* (3), 558–571.

(17) Yamane, T.; Murakami, S.; Ikeguchi, M. Functional Rotation Induced by Alternating Protonation States in the Multidrug Transporter AcrB: All-Atom Molecular Dynamics Simulations. *Biochemistry* **2013**, *52* (43), 7648–7658.

(18) Mitchell, M. R.; Tlusty, T.; Leibler, S. Strain Analysis of Protein Structures and Low Dimensionality of Mechanical Allosteric Couplings. *Proc. Natl. Acad. Sci. U. S. A.* **2016**, *113* (40), E5847–E5855.

(19) Leitner, D. M.; Yamato, T. Mapping Energy Transport Networks in Proteins. In *Reviews in Computational Chemistry*; Parrill, A. L., Lipkowitz, K. B., Eds.; John Wiley & Sons, Inc.: New York, 2018; Vol. 31, pp 63–113.

(20) Leitner, D. M. Energy Flow in Proteins. *Annu Rev Phys Chem* **2008**, *59*, 233–259.

(21) *Proteins: Energy, Heat and Signal Flow*; Leitner, D. M., Straub, J. E., Eds.; CRC Press, 2009.

(22) Takayanagi, M.; Okumura, H.; Nagaoka, M. Anisotropic Structural Relaxation and Its Correlation with the Excess Energy Diffusion in the Incipient Process of Photodissociated MbCO: High-Resolution Analysis via Ensemble Perturbation

Method. *J. Phys. Chem. B* **2007**, *111* (4), 864–869.

(23) Xu, Y.; Leitner, D. M. Communication Maps of Vibrational Energy Transport Through Photoactive Yellow Protein. *J. Phys. Chem. A* **2014**, *118* (35), 7280–7287.

(24) Leitner, D. M. Frequency-Resolved Communication Maps for Proteins and Other Nanoscale Materials. *J. Chem. Phys.* **2009**, *130* (19).

(25) Buchenberg, S.; Leitner, D. M.; Stock, G. Scaling Rules for Vibrational Energy Transport in Globular Proteins. *J. Phys. Chem. Lett.* **2016**, *7* (1), 25–30.

(26) Reid, K. M.; Yamato, T.; Leitner, D. M. Scaling of Rates of Vibrational Energy Transfer in Proteins with Equilibrium Dynamics and Entropy. *J. Phys. Chem. B* **2018**, *122* (40), 9331–9339.

(27) Ishikura, T.; Yamato, T. Energy Transfer Pathways Relevant for Long-Range Intramolecular Signaling of Photosensory Protein Revealed by Microscopic Energy Conductivity Analysis. *Chem. Phys. Lett.* **2006**, *432* (4–6), 533–537.

(28) Ishikura, T.; Iwata, Y.; Hatano, T.; Yamato, T. Energy Exchange Network of Inter-Residue Interactions within a Thermally Fluctuating Protein Molecule: A

Computational Study. *J. Comput. Chem.* **2015**, *36* (22), 1709–1718.

(29) Hoch, J. A. Two-Component and Phosphorelay Signal Transduction. *Curr. Opin. Microbiol.* **2000**, *3* (2), 165–170.

(30) Stock, A. M.; Robinson, V. L.; Goudreau, P. N. Two-Component Signal Transduction. *Annu. Rev. Biochem.* **2000**, *69* (1), 183–215.

(31) Ayers, R. A.; Moffat, K. Changes in Quaternary Structure in the Signaling Mechanisms of PAS Domains. *Biochemistry* **2008**, *47* (46), 12078–12086.

(32) Gilles-Gonzalez, M. A.; Gonzalez, G.; Perutz, M. F.; Kiger, L.; Marden, M. C.; Poyart, C. Heme-Based Sensors, Exemplified by the Kinase FixL, Are a New Class of Heme Protein with Distinctive Ligand Binding and Autoxidation. *Biochemistry* **1994**, *33* (26), 8067–8073.

(33) Wright, G. S. A.; Saeki, A.; Hikima, T.; Nishizono, Y.; Hisano, T.; Kamaya, M.; Nukina, K.; Nishitani, H.; Nakamura, H.; Yamamoto, M.; et al. Architecture of the Complete Oxygen-Sensing FixL-FixJ Two-Component Signal Transduction System. *Sci. Signal.* **2018**, *11* (525).

(34) Möglich, A.; Ayers, R. A.; Moffat, K. Addition at the Molecular Level: Signal

Integration in Designed Per-ARNT-Sim Receptor Proteins. *J. Mol. Biol.* **2010**, *400* (3), 477–486.

(35) Möglich, A.; Ayers, R. A.; Moffat, K. Design and Signaling Mechanism of Light-Regulated Histidine Kinases. *J. Mol. Biol.* **2009**, *385* (5), 1433–1444.

(36) Diensthuber, R. P.; Bommer, M.; Gleichmann, T.; Möglich, A. Full-Length Structure of a Sensor Histidine Kinase Pinpoints Coaxial Coiled Coils as Signal Transducers and Modulators. *Structure* **2013**, *21* (7), 1127–1136.

(37) Bhate, M. P.; Molnar, K. S.; Goulian, M.; DeGrado, W. F. Signal Transduction in Histidine Kinases: Insights from New Structures. *Structure* **2015**, *23* (6), 981–994.

(38) Casino, P.; Rubio, V.; Marina, A. The Mechanism of Signal Transduction by Two-Component Systems. *Curr. Opin. Struct. Biol.* **2010**, *20* (6), 763–771.

(39) Casino, P.; Rubio, V.; Marina, A. Structural Insight into Partner Specificity and Phosphoryl Transfer in Two-Component Signal Transduction. *Cell* **2009**, *139* (2), 325–336.

(40) Berntsson, O.; Diensthuber, R. P.; Panman, M. R.; Björling, A.; Gustavsson, E.;

Hoernke, M.; Hughes, A. J.; Henry, L.; Niebling, S.; Takala, H.; et al. Sequential Conformational Transitions and α-Helical Supercoiling Regulate a Sensor Histidine Kinase. *Nat. Commun.* **2017**, *8* (1), 284.

(41) Berntsson, O.; Diensthuber, R. P.; Panman, M. R.; Björling, A.; Hughes, A. J.; Henry, L.; Niebling, S.; Newby, G.; Liebi, M.; Menzel, A.; et al. Time-Resolved X-Ray Solution Scattering Reveals the Structural Photoactivation of a Light-Oxygen-Voltage Photoreceptor. *Structure* **2017**, *25* (6), 933–938.e3.

(42) Engelhard, C.; Diensthuber, R. P.; Möglich, A.; Bittl, R. Blue-Light Reception through Quaternary Transitions. *Sci. Rep.* **2017**, *7* (1), 1385.

(43) Yamato, T.; Niimura, N.; Go, N. Molecular Dynamics Study of Femtosecond Events in Photoactive Yellow Protein after Photoexcitation of the Chromophore. *Proteins* **1998**, *32* (3), 268–275.

(44) Yamada, A.; Ishikura, T.; Yamato, T. Direct Measure of Functional Importance Visualized Atom-by-Atom for Photoactive Yellow Protein: Application to Photoisomerization Reaction. *Proteins* **2004**, *55* (4), 1070–1077.

(45) Yamada, A.; Ishikura, T.; Yamato, T. Role of Protein in the Primary Step of the

Photoreaction of Yellow Protein. *Proteins* **2004**, *55* (4), 1063–1069.

(46) Koike, K.; Kawaguchi, K.; Yamato, T. Stress Tensor Analysis of the Protein Quake of Photoactive Yellow Protein. *Phys Chem Chem Phys* **2008**, *10* (10), 1400–1405.

(47) Yamada, A.; Yamamoto, S.; Yamato, T.; Kakitani, T. Ab Initio MO Study on Potential Energy Surfaces for Twisting around C7□C8 and C4–C7 Bonds of Coumaric Acid. *J. Mol. Struct. THEOCHEM* **2001**, *536* (2–3), 195–201.

(48) Key, J.; Moffat, K. Crystal Structures of Deoxy and CO-Bound BjFixLH Reveal Details of Ligand Recognition and Signaling. *Biochemistry* **2005**, *44* (12), 4627–4635.

(49) Gong, W.; Hao, B.; Chan, M. K. New Mechanistic Insights from Structural Studies of the Oxygen-Sensing Domain of Bradyrhizobium Japonicum FixL. **2000**, 3955–3962.

(50) Case, D. A.; Babin, V.; Berryman, J. T.; Betz, R. M.; Cai, Q.; Cerutti, D. S.; Cheatham, T. E.; Darden, T. A.; Duke, R. E.; Gohlke, H.; et al. *Amber 14* - *University of California, San Francisco*; 2014.

(51) Maier, J. A.; Martinez, C.; Kasavajhala, K.; Wickstrom, L.; Hauser, K. E.; Simmerling, C. Ff14SB: Improving the Accuracy of Protein Side Chain and Backbone Parameters from Ff99SB. *J. Chem. Theory Comput.* **2015**, *11* (8), 3696–3713.

(52) Jorgensen, W. L.; Chandrasekhar, J.; Madura, J. D.; Impey, R. W.; Klein, M. L. Comparison of Simple Potential Functions for Simulating Liquid Water. *J. Chem. Phys.* **1983**, *79* (2), 926.

(53) Giammona, D. Ph. D. Thesis, University of California, 1984.

(54) Henry, E. R.; Levitt, M.; Eaton, W. A. Molecular Dynamics Simulation of Photodissociation of Carbon Monoxide from Hemoglobin. *Proc. Natl. Acad. Sci.* **1985**, *82* (7), 2034–2038.

(55) Frish, M. J.; Trucks, G. W.; Schlegel, H. B.; Scuseria, G. E.; Robb, M. A.; Cheeseman, J. R. Gaussian 03. *Gaussian Inc, Wallingford CT* **2003**.

(56) Schaftenaar, G.; Noordik, J. H. Molden: A Pre- and Post-Processing Program for Molecular and Electronic Structures*. *J. Comput. Aided. Mol. Des.* **2000**, *14* (2), 123–134.

(57) Dupradeau, F.-Y.; Pigache, A.; Zaffran, T.; Savineau, C.; Lelong, R.; Grivel, N.; Lelong, D.; Rosanski, W.; Cieplak, P. The R.E.D. Tools: Advances in RESP and ESP Charge Derivation and Force Field Library Building. *Phys. Chem. Chem. Phys.* **2010**, *12* (28), 7821–7839.

(58) Ishikura, T.; Hatano, T.; Yamato, T. Atomic Stress Tensor Analysis of Proteins. *Chem. Phys. Lett.* **2012**, *539*, 144–150.

(59) Yamato, T. Strain Tensor Field in Proteins. *J. Mol. Graph.* **1996**, *14* (2), 105–107, 98–99.

(60) Lee, B.; Richards, F. M. The Interpretation of Protein Structures: Estimation of Static Accessibility. *J. Mol. Biol.* **1971**, *55* (3), 379–400.

(61) Tuckerman, J. R.; Gonzalez, G.; Dioum, E. M.; Gilles-Gonzalez, M.-A. Ligand and Oxidation-Site Specific Regulation of the Heme-Based Oxygen Sensor FixL from Sinorhizobium Melitloti. *Biochemistry* **2002**, *41*, 6170–6177.

(62) Gilles-Gonzalez, M. A.; Caceres, A. I.; Sousa, E. H. S.; Tomchick, D. R.; Brautigam, C.; Gonzalez, C.; Machius, M. A Proximal Arginine R206 Participates in Switching of the Bradyrhizobium Japonicum FixL Oxygen

Sensor. *J. Mol. Biol.* **2006**, *360* (1), 80–89.

(63) Gong, W.; Hao, B.; Mansy, S. S.; Gonzalez, G.; Gilles-Gonzalez, M. a; Chan, M. K. Structure of a Biological Oxygen Sensor: A New Mechanism for Heme-Driven Signal Transduction. *Proc. Natl. Acad. Sci. U. S. A.* **1998**, *95* (26), 15177–15182.

(64) Perutz, M. F.; Paoli, M.; Lesk, A. M. FixL, a Haemoglobin That Acts as an Oxygen Sensor: Signalling Mechanism and Structural Basis of Its Homology with PAS Domains. *Chem. Biol.* **1999**, *6* (11), R291--R297.

(65) Mukai, M.; Nakamura, K.; Nakamura, H.; Iizuka, T.; Shiro, Y. Roles of Ile209 and Ile210 on the Heme Pocket Structure and Regulation of Histidine Kinase Activity of Oxygen Sensor FixL from Rhizobium Meliloti. *Biochemistry* **2000**, *39* (45), 13810–13816.

(66) Miyatake, H.; Mukai, M.; Park, S. Y.; Adachi, S.; Tamura, K.; Nakamura, H.; Nakamura, K.; Tsuchiya, T.; Iizuka, T.; Shiro, Y. Sensory Mechanism of Oxygen Sensor FixL from Rhizobium Meliloti: Crystallographic, Mutagenesis and Resonance Raman Spectroscopic Studies. *J. Mol. Biol.* **2000**, *301* (2), 415–431.

(67) Dunham, C. M.; Dioum, E. M.; Tuckerman, J. R.; Gonzalez, G.; Scott, W. G.; Gilles-Gonzalez, M. A. A Distal Arginine in Oxygen-Sensing Heme-PAS Domains Is Essential to Ligand Binding, Signal Transduction, and Structure. *Biochemistry* **2003**, *42* (25), 7701–7708.

(68) Miyatake, H.; Mukai, M.; Park, S.-Y.; Adachi, S.; Tamura, K.; Nakamura, H.; Nakamura, K.; Tsuchiya, T.; Iizuka, T.; Shiro, Y. Sensory Mechanism of Oxygen Sensor FixL from Rhizobium Meliloti: Crystallographic, Mutagenesis and Resonance Raman Spectroscopic Studies11Edited by K. Nagai. *J. Mol. Biol.* **2000**, *301* (2), 415–431.

(69) Yano, S.; Ishikawa, H.; Mizuno, M.; Nakamura, H.; Shiro, Y.; Mizutani, Y. Ultraviolet Resonance Raman Observations of the Structural Dynamics of Rhizobial Oxygen Sensor FixL on Ligand Recognition. *J. Phys. Chem. B* **2013**, *117* (49), 15786–15791.

(70) Yamawaki, T.; Ishikawa, H.; Mizuno, M.; Nakamura, H.; Shiro, Y.; Mizutani, Y. Regulatory Implications of Structural Changes in Tyr201 of the Oxygen Sensor Protein FixL. *Biochemistry* **2016**, *55* (29), 4027–4035.

(71) Gilles-Gonzalez, M. A.; Gonzalez, G. Heme-Based Sensors: Defining Characteristics, Recent Developments, and Regulatory Hypotheses. *J. Inorg. Biochem.* **2005**, *99* (1), 1–22.

(72) Sousa, E. H. S.; Tuckerman, J. R.; Gondim, A. C. S.; Gonzalez, G.; Gilles-Gonzalez, M. A. Signal Transduction and Phosphoryl Transfer by a FixL Hybrid Kinase with Low Oxygen Affinity: Importance of the Vicinal PAS Domain and Receiver Aspartate. *Biochemistry* **2013**, *52* (3), 456–465.

(73) Casino, P.; Rubio, V.; Marina, A. The Mechanism of Signal Transduction by Two-Component Systems. *Curr. Opin. Struct. Biol.* **2010**, *20* (6), 763–771.

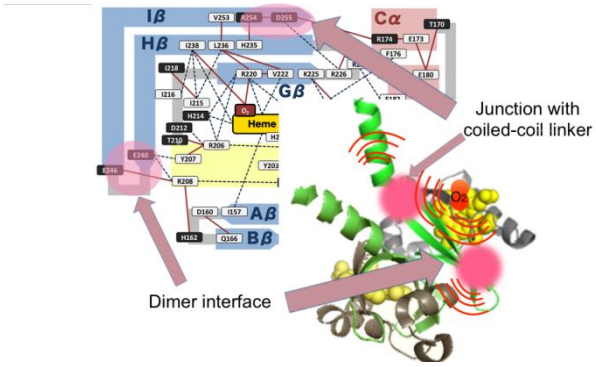
Iβ
Hβ
Gβ
Cα
Aβ
Bβ
Heme
Junction with
coiled-coil linker
Dimer interface

TOC IMAGE